Computer Aided Analysis of Filament Wound Composite Pressure Vessel with Integrated End Domes considering the Change of Winding Angles through the Thickness Direction

M Madhavi, *Non-member*
Dr K V J Rao, *Fellow*

Filament -wound composite pressure vessels are an important high-pressure container, widely applied in the commercial and aerospace industries. The determination of a proper winding angle and thickness is very important to decrease manufacturing difficulties and to increase structural efficiency. In this study, possible winding angles considering the slippage between a fibre and a mandrel surface are calculated using geodesic and semi-geodesic path equations. Netting analysis is used for the calculation of hoop and helical thickness of the shell. A balanced symmetric ply sequence for carbon T300/epoxy is considered for the entire pressure vessel. Finite element analyses were performed considering the change of winding angles through the thickness by a commercial FEA code, ANSYS. Different filament wound end domes, ie, hemi-spherical, isotensoid (geodesic), constant deviation line (non-geodesic) structures considered for continuous change of the winding angle and thickness at the dome part due to fibre built-up near the metallic boss. Finite element analysis, can predict the deformation of filament wound structures. The results can be utilized to understand structural characteristics of filament wound pressure vessels with integrated end domes. Membrane stresses and radial deformations are compared with finite element results for all the three type of domes. Also the theoretical result of stress in the fibre direction of the optimum end dome is compared to that of finite element results.

Keywords: Filament winding; Fibre slippage; Pole opening; Netting analysis

INTRODUCTION

Filament-wound composite pressure vessels, which utilize a fabrication technique of filament winding, (Figure 1) to form high strength and light weight reinforced plastic parts, are a major type high-pressure vessel and widely used in the commercial and aerospace industries such as fuel tanks, portable oxygen storage, rocket motor cases and so on. These vessels consists of a cylindrical drum and dome parts, just like typical pressure vessels. Since filament-wound composite pressure vessels are apt to fail in their dome parts, the design of the dome parts is the first issue in the design of filament -wound composite pressure vessels. Several considerations must be given to dome contours, including the strength of selected materials, the effect of end openings, winding stability, geometric variables and so on. The winding patterns and dome shapes must be carefully chosen to achieve an optimum. The trajectory of the fibre path and the corresponding fibre angles cannot be chosen arbitrarily because of the stability requirement.

The fibre path instability induced by fibre slippage on a mandrel surface is too complicated to be predicted because it is affected by many parameters, such as temperature, mandrel shape, fibre-resin combination, surface treatment and so on.

Isotensoid dome design, constant deviation line dome design and spherical wound dome design have been used to determine the winding patterns and dome geometry of pressure vessels. An isotensoid vessel is assumed to support internal pressure by the fibre only, which consist of filaments that are loaded to an identical stress level. Whereas, non-geodesic end dome design is considered for

M Madhavi is with the Maturi Venkata Subba Rao Engineering College, Nadergul, Hyderabad 501 510 and Dr K V J Rao is with the St. Martins Engineering College, Quthbullapur, Secunderbad 500 014.

This paper (modified) was received on August 11, 2008. Written discussion on this paper will be entertained upto June 30, 2010.

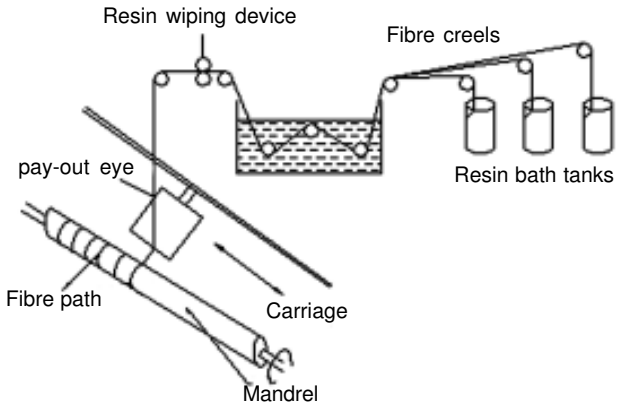

Figure 1 Schematic sketch of filament winding technique

the vessels with unequal openings, *ie*, rocket motor case. The fibre path depends on the surface where the fibres are wound and the shape of the surface is changing with already built-up fibres as the filament winding process is carried out. Especially the surface change during the winding process becomes relatively large because the thickness is higher near the polar opening than in the other dome parts, which should not be ignored. Therefore the fibre angle must be calculated in the thickness direction to consider the changed shape of the dome surface during the winding process even at the same axial position of the dome region.

In the present study, hoop and helical thickness are calculated using netting analysis and fibre angle distribution for both cylinder and end domes are calculated using Claurit's principle for the geodesic domes. Geodesic lines connect two points along the shortest distance over the surface. In this case no friction force is required to keep the fibre from slipping, since it follows a self-stable trajectory. The non-geodesic path is slightly deviating from the geodesic path counting on friction to keep the fibre in its proper position. Geometrically non-linear finite element analyses considering the change of winding angles through the thickness were performed.

THEORITICAL BACKGROUND

The composite pressure vessel consists of a durable plastic liner fully wrapped with epoxy-impregnated carbon fibre as shown in Figure 2. The liner is formed from high-density polyethylene (HDPE) and has two aluminum end bosses, which provide the structural interface to the shell. The function of the liner is to provide a high-pressure gas barrier. The liner is not considered as a structural element of design and, by virtue of its low modulus, is able to transfer all loads to the structural shell. The composite pressure vessel has a base radius of '*a*' and polar opening radius of 'r_0', Such a dome is formed by winding a resin coated high strength filament on an axisymmetric permanent lining or removable mandrel, then heat treating the resulting structure to produce a hard and resistance matrix. The filament patterns produced by the manufacturing methods consist of superimposed layers sustains with alternate spiral, so that each clockwise-wound layer exists. The double symmetry of the resulting pattern is adopted herein, and the dome is generally treated as a thin-walled shell of revolution. The shell is subjected to uniform internal pressure and the conditions of thin walled structure and balanced symmetry winding pattern are adopted. Herein the force resultants are derived based on membrane theory and the stress-strain relationships are analyzed using classical laminated theory.

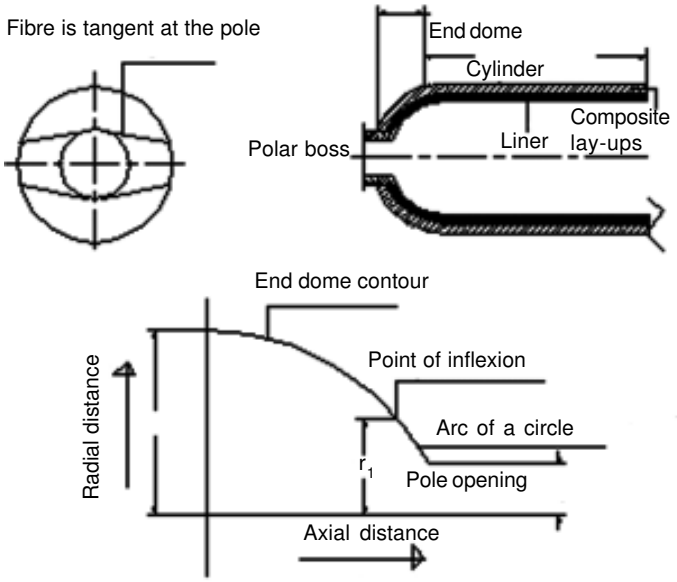

Figure 2 Composite pressure vessel with integrated end domes with varying thickness, t and lay-up angles, θr along the radius

Geometrical Relations

Composite pressure vessels are fabricated by winding threads or tapes impregnated with epoxy resin onto a properly shaped mandrel. Consider a shell of revolution consisting of K composite layers, each layer being reinforced by fibres oriented at angles $+\phi_l$ and $-\phi_l$ to the meridian[1]. The shell is loaded by a uniform internal pressure p and axial forces Q_0, distributed uniformly over the edge of the polar opening with radius r_0, shown in Figure 3. Let R_1 and R_2 are principal radii of curvature.

Force Resultants

The internal force resultants of the dome are evaluated using the membrane theory. From the force equilibrium equations of the dome element, the force resultants are given by

$$\frac{N_{1i}}{R_1} + \frac{N_{2i}}{R_2} = P \qquad (1)$$

The dome surface is symmetrically loaded with respect to its axis. The deformations will be symmetrical with respect to this axis and thus the shear force $N_{12i} = 0$

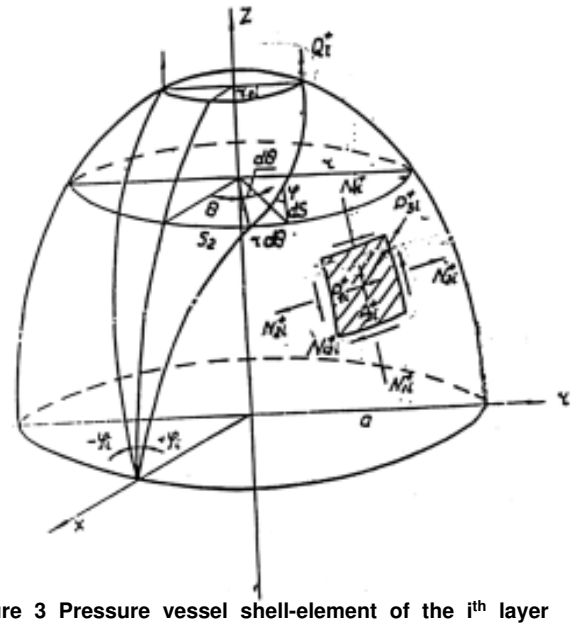

Figure 3 Pressure vessel shell-element of the ith layer

$$\frac{1}{R_1} = \frac{Z''}{\left(1 + Z'^2\right)^{3/2}}$$

$$\text{or } \frac{1}{R_2} = \frac{Z'}{r\left(1 + Z'^2\right)^{1/2}} \quad (2)$$

Where primes denote differentiation with respect to Z.

Governing Equation

The governing system of equations for the meridian shape and coordinates of the fibres are denoted as

$$\frac{d^2Z}{dr^2} = \frac{2rZ'[1 + (Z')^2]}{r^2 - r_o^2} - \frac{Z'\xi^2[1 + (Z')^2]}{r(r^2 - \xi^2)} \quad (3)$$

$$\frac{d\xi}{dr} = \frac{\pm 2Z'(r^2 - \xi^2)\mu}{r^2 - r_o^2} \quad (4)$$

The boundary conditions are, $r = a$, $Z = 0$, $1/Z' = 0$,

$\xi = \xi_a$, where $\xi = r\sin\varphi$

Further, a is the radius of the cylinder; r_i, variable radius; r_0, pole opening radius and μ, friction factor on the mandrel surface.

If $\mu = 0$, the condition is satisfied for isotensoid equation, where as $\mu \neq 0$ for non-geodesic equation.

Classical Lamination Theory

The constitutive equations for a symmetric angle plylaminate, where each layer has the same thickness as

$$\begin{bmatrix}\sigma_{1i}\\ \sigma_{2i}\\ \sigma_{12i}\end{bmatrix} = \begin{bmatrix}C_{11} & C_{12} & 0\\ C_{12} & C_{22} & 0\\ 0 & 0 & C_{33}\end{bmatrix}\begin{bmatrix}\varepsilon_{1i}\\ \varepsilon_{2i}\\ \varepsilon_{12i}\end{bmatrix}$$

$C_{11} = Q_{11}\, l^4 + 2\,(Q_{12} + 2Q_{33}) l^2 m^2 + Q_{22}\, m^4$

$C_{12} = (Q_{11}\, l^4 + Q_{22} - 4Q_{33})\, l^2 m^2 + Q_{22}\,(l^4 + m^4)$

$C_{22} = Q_{11} m^4 + 2(Q_{12} + 2Q_{33})\, l^2 m^2 + Q_{22}\, l^4$

$C_{33} = 2(Q_{11} + Q_{12} - 2Q^{12} - 2Q^{33})\, l^2 m^2 + Q_{33}\,(l^4 + m^4)$

Where $\cos\varphi = l$ and $\sin\varphi = m$ as determined by R M Jones[2].

The terms C_{11}, C_{12}, C_{33} are the laminate stiffness coefficients in the meridian, σ_{1i}, hoop σ_{2i} and σ_{12i} shear directions, respectively. The stiffness coupling is denoted by C_{12} strictly between the meridian and hoop direction. The filament wound structures are not symmetric, but alternating plus, minus plies, and multiple plus/minus layers results the quickly fade non symmetric aspect of the laminates. It is assumed that C_{13} and C_{23} are zero.

Shell Membrane Stresses in Material Coordinate System

Stresses in the local material coordinate system particularly in the fibre direction, are designed to determine the failure mode of composite laminate shell[3].

$$\begin{bmatrix}\sigma_f\\ \sigma_t\\ \sigma_{ft}\end{bmatrix} = \begin{bmatrix}Q_{11} & Q_{12} & 0\\ Q_{12} & Q_{22} & 0\\ 0 & 0 & Q_{33}\end{bmatrix}\left[\begin{bmatrix}\overline{l^2} & \overline{m^2}\\ m^2 & l^2\\ -ml & ml\end{bmatrix}\right]\begin{bmatrix}\varepsilon_{1i}\\ \varepsilon_{2i}\\ \varepsilon_{12i}\end{bmatrix}$$

The shear stress $\sigma_{12i} = 0$; The local stresses, in terms of the strains are :

$$\begin{bmatrix}\varepsilon_{1i}\\ \varepsilon_{2i}\end{bmatrix} = \begin{bmatrix}S_{11} & S_{12}\\ S_{12} & S_{22}\end{bmatrix}\begin{bmatrix}\sigma_{1i}\\ \sigma_{2i}\end{bmatrix}$$

$S_{11} = C_{22} / (C_{11}\, C_{12} - C_{12}^2)$; $S_{22} = C_{11} / (C_{11}\, C_{22} - C_{12}^2)$

$S_{12} = C_{12} / (C_{11}\, C_{22} - C_{12}^2)$; $S_{33} = 1/\, C_{33}$

The final stress in the fibre direction is

$$\sigma_f = \frac{\left(Q_{11}l^2 + Q_{12}m^2\right)\left(C_{22}\sigma_{1i} - C_{12}\sigma_{2i}\right) + \left(Q_{11}m^2 + Q_{12}l^2\right)\left(C_{11}\sigma_{1i} - C_{12}\sigma_{2i}\right)}{\left(C_{11}C_{22} - C_{12}^2\right)} \quad (5)$$

Tsai-Wu Failure Criterion

To assess the strength of the dome structure, a failure criterion is needed. Some bi-axial failure criteria for orthotropic lamina include the maximum stress criterion, the maximum strain criterion, the Tsai-Hill failure criterion and the Tsai-Wu failure criterion. No interaction exists between the failure modes in the maximum stress and the maximum strain criterion. Meanwhile, some faults certainly exist for the orthotropic lamina with the Tsai-Hill failure criterion[2]. To avoid both tensile failure transverse to fibres and shear failure along fibres, the design against failure is determined by employing the Tsai-Wu tensor failure criterion herein. Specific merits of the Tsai-Wu tensor include, invariance under rotation, transformation via known tensor transformation laws and symmetry properties akin to those of the stiffness and compliance. The Tsai-Wu failure criterion stipulates that for nonfailure the constraint ($k - k^{th}$ layer),

$F11\ (s1i^{(k)})^2 + F_{22}\,(\sigma_{2i}^{(k)})^2 + F_{66}\,(\sigma_{12i}^{(k)})^2 + 2F_{12}\,\sigma_{2i}^{(k)}\,\sigma_{1i}^{(k)} + F_1\,(\sigma_{1i}^{(k)}) + F_2\,(\sigma_{2i}^{(k)}) - 1 < 0;$

Should be satisfied (6)

The strength parameters F_{11}, F_{22}, F_{66}, F_1, F_2 are given by

$F_{11} = 1/\sigma_{1iu}\,\sigma_{1iu}'$; $F_{22} = 1/\sigma_{2iu}\,\sigma_{2iu}'$; $F_{66} = 1/\sigma^2_{12iu}$; $F_1 = 1/\sigma_{1iu} - 1/\sigma_{1iu}'$; $F_2 = 1/\sigma_{2iu} - 1/\sigma_{2iu}'$;

$F_{12} = 1/\,(2\,(\sigma_{1i\,u}\,\sigma_{1iu}'\,\sigma_{2iu}\,\sigma_{2iu}')^{1/2})$

Where $\sigma_{1i\,u}$, σ_{1iu}', σ_{2iu}, σ_{2iu}' are the tensile and compressive strengths of the composite material in the longitudinal and transverse directions, and σ_{12iu} is the in-plane shear strength.

Winding Condition

Geodesic winding involves having windings go along the shortest distance between two points on the winding surface to ensure structural stability, that is, no slipping and no bending between the filaments and the winding surface. This study considers the geodesic condition in which Clairut's equation is satisfied. As per the conditions, $r\sin\phi$ = constant, where ϕ -is the winding angle between a filament and a meridian line in a point on the surface, and r is the radial distance to the axis of rotation Z. The fibres paths are taken as tangential to the polar opening. At the tangency point, winding angle ϕ equals $\pi/2$, and thus for a opening radius r_0, then $\sin\phi = r_0 / r$.

Although a filament wound pressure vessel generally represents a thin-walled structure and the wall consists of several layers. For a given radius r_0 the winding angle ϕ depends on the radial distance r. The angle ϕ will change over the thickness of the wall. Herein, this change is assumed to be negligible, so all layers are wound alternately $+\phi$ and $-\phi$ at a certain point of the meridian line. Additionally, assuming that each filament crosses the equator and all other parallel circles in the dome an equal number of fibres, that is, the filaments do not terminate or double back, one finds that

$$t\,(2\,\pi r)\cos\phi = t_c\,(2\,\pi r_c)\,\cos\phi_c = \text{constant} \qquad (7)$$

Where t, r, ϕ, respectively, denote the shell thickness, radius and winding bangle of a parallel circle plane of Z=constant[4].

Thickness Calculation

The cylinder of the filament wound pressure vessel was basically composed of helical and hoop layers. The preliminary design is performed using netting analysis methods to address the inner pressure loading. Netting analysis assumes that the fibres provide all of the stiffness and strength in the cylinder. This assumption is not only conservative but also an excellent basis for quick calculation of composite thickness. From netting analysis[5].

$$\sigma_{f\,\varphi} = PR / (2\,t_{helical})_{FRP}\,(V_f)_{helical}\cos^2\phi) \qquad (8)$$

$$\sigma_{fH} = PR/\left(t_{hoop}\right)_{FRP}\left(V_f\right)_{hoop}\left\{1-\left(\tan^2\phi\right)/2\right\} \qquad (9)$$

and the stress ratio $= \sigma_{f\varphi}/\sigma_{fH} = \left(t_{hoop}\right)_{FRP}/$

$$\left(t_{helical}\right)_{FRP}\left\{\frac{1}{2\cos^2\phi-\sin^2\phi}\right\}$$

when σ_f, σ_{fH} are the fibre strength in helical and hoop layer, respectively, ϕ, helical winding angle, $(V_f)_{helical}$, $(V_f)_{hoop}$), fibre volume fraction in helical and hoop ply respectively, R, is the inner radius of pressure vessel. To prevent the failure in the dome or by boss blowout, the pressure vessels were designed with 0.8 stress ratio[5].

Analysis of the End Domes

The non-linear differential equation of end dome contours given in equation (3) are solved by fourth order Runga-Kutta method and C-programme is used to develop co-ordinates of the dome contours[6] as shown in Figure 4. For all practical purposes : i) $\phi_0 < \phi < 54.7^o$, the shape of the contours is either geodesic or non-geodesic. As the filament leaves the dome and continues over the polar ring, the wind angle increases to 90^o as the fibre becomes tangent to the polar opening. ii) $54.70 < \phi < 90^o$, the head is spherical, (or frustum of a cone) and its radius being equal to the value taken by r_i at the point of inflexion (it is a point where the curvature taken a reverse direction). iii) The value $\mu = 0$ for isotensoid and $\mu = 0.2$ for non-geodesic domes is considered in this study[7]. After determining the winding angle values and helical -hoop thickness by netting analysis, the ply sequence is calculated using balanced symmetric lamination[8–10]. The ply sequences along with the thickness at different zones of the domes are shown in the Table 1 to Table 3. The stress along the fibre is studied through FEA and the stress distribution for different contours are shown from Figure 5 to Figure 7. Behavior of three end domes like isotensoid, nongeodesic, spherical end domes are considered for the study with pole opening of, r_0 = 125 mm and cylindrical radius, a = 593 mm, subjected to uniform internal pressure of 7.5 Mpa, shown in the Figure 8 to Figure 12. The hoop strength and helical strength of the carbonT300/epoxy found from material characterization are,

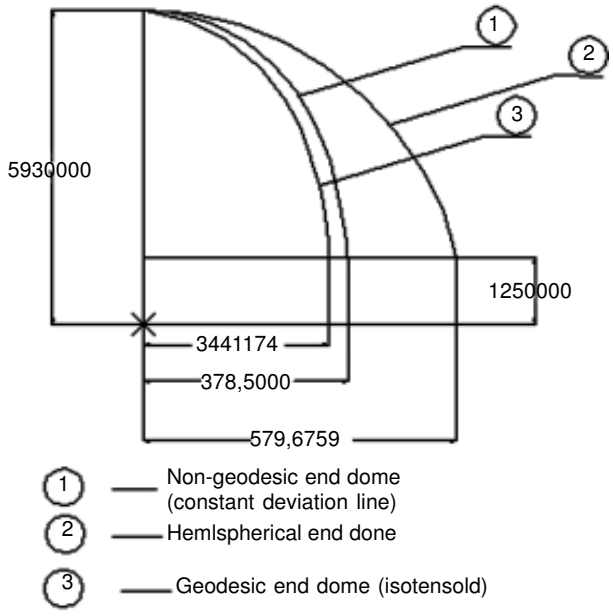

Figure 4 Comparison of end dome profiles

Table 1 Ply sequence of isotensoid end dome (r_0 = 125 mm)

R mm	φ º	Total Thickness, mm	Ply sequence (hoop and helical winding patterns)
593	12.17	6.04	$[90/+\varphi_1/-\varphi_1/90/+\varphi_1/-\varphi_1/90]_S$
592	12.19	9.64	
557	12.97	9.82	$[90/+\varphi_2/-\varphi_2/90/+\varphi_2/-\varphi_2/90]_S$
497	14.56	10.26	
432	16.82	11.03	$[90/+\varphi_3/-\varphi_3/90/\varphi_3/-\varphi_3]_S$
377	19.36	12.03	
307	24.02	14.19	$[90/+\varphi_4/-\varphi_4/+\varphi_4/-\varphi_4/90]_S$
252	29.73	17.29	
207	37.14	22.09	$[90/+\varphi_5/-\varphi_5/+\varphi_5/-\varphi_5]_S$
177	44.92	28.44	
152	55.32	40.36	$[+\varphi_6/-\varphi_6/+\varphi_6/-\varphi_6/90]_S$
125	90	45	

Table 2 Ply sequence of non-geodesic end dome (r_0 = 125 mm)

R, mm	φ, º	Total thickness, mm	Ply sequence (hoop and helical winding patterns)
125	90	20	$[+\varphi_7/-\varphi_7/+\varphi_7/-\varphi_7]_S$
153.7	54.73	16.9	
172	47.11	13.25	$[+\varphi_6/-\varphi_6/+\varphi_6/-\varphi_6/90]_S$
229.47	31.83	8.88	
314.4	25.19	7.03.	$[90/+\varphi_5/-\varphi_5/+\varphi_5/-\varphi_5/90]_S$
381.9	21.85	6.43	
473	19.91	6.14	$[90/+\varphi_4/-\varphi_4/90/+\varphi_4/-\varphi_4]_S$
533.7	20.01	6.11	
574.9	21.23	6.13	$[90/+\varphi_3/-\varphi_3/90/+\varphi_3/-\varphi_3/90]_S$
593	23.99	6.1	$[90/+\varphi_2/-\varphi_2/90/+\varphi_2/-\varphi_2/90]_S$
593	24.17	6.1	$[90/+\varphi_1/-\varphi_1/90/+\varphi_1/-\varphi_1/90]_S$
593	24.34	6.1	

Table 3 Ply sequence of spherical end dome (r_0 = 125 mm)

R, mm	φ, º	Total thickness, mm	Ply sequence (hoop and helical winding patterns)
593	12.16	6.011	$[90/+\varphi_1/-\varphi_1/90/+\varphi_1/-\varphi_1/90]_S$
584.4	12.35	9.68	
562.5	12.83	9.74	$[90/+\varphi_2/-\varphi_2/90/+\varphi_2/-\varphi_2/90]_S$
525.19	13.76	9.98	
478.3	15.14	10.39	$[90/+\varphi_3/-\varphi_3/90/+\varphi_3/-\varphi_3]_S$
423.02	17.18	11.11	
370.06	19.74	12.14	$[90/+\varphi_4/-\varphi_4/+\varphi_4/-\varphi_4/90]_S$
298.74	24.73	14.68	
224.24	33.87	20.09	$[+\varphi_5/-\varphi_5/+\varphi_5/-\varphi_5/90]_S$
153.5	55.52	40.09	
125	90	45.67	$[+\varphi_6/-\varphi_6/+\varphi_6/-\varphi_6/90]_S$

1.2 GPa and 0.96 GPa, respectively. The material properties of carbonT300/epoxy used for the analysis are: E_1 = 144 GPa; E_2 = 6.5 GPa; E_3 = 6.5 GPa; G_{12} = 5.6 GPa; G_{23} = 2.6 GPa; G_{31} = 2.6 GPa; γ_{12} = 0.2; γ_{23} = 0.32; γ_{31} = 0.0096; V_f = 0.6; V_m = 0.4, which are discussed[11–13]. The layered composite 3-D shell-99 shell element is a more developed element and has more capabilities to model filament wound layered structures. The model is extruded for 30º

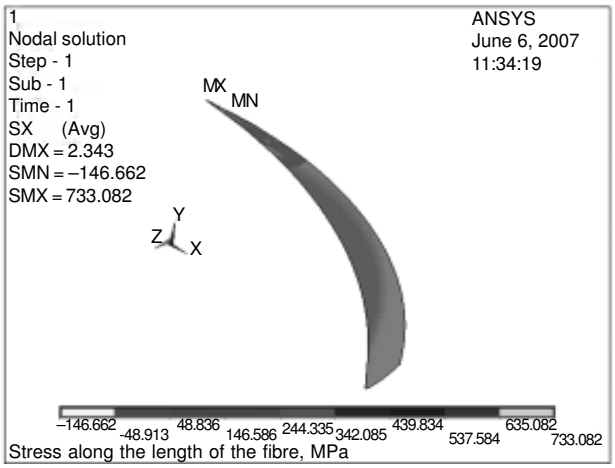

Figure 5 Stress along the fiber for isotensoid end dome

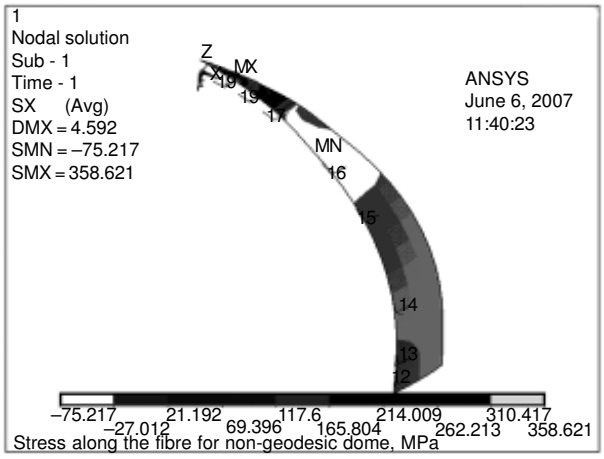

Figure 6 Stress along the fiber for non-geodesic end dome

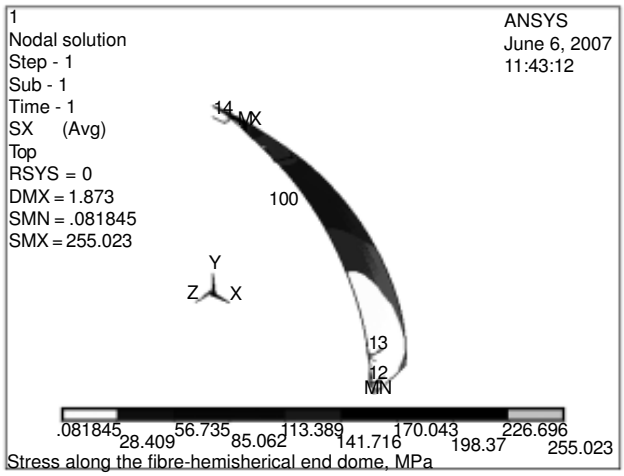

Figure 7 Stress along the fiber for Hemi-spherical end dome

orientations and the analysis is performed. The domes are divided into zones and in each zone the material and geometrical properties are incorporated into the layers of the element.

RESULT AND DISCUSSIONS

In designing composite pressure vessels, emphasis is laid

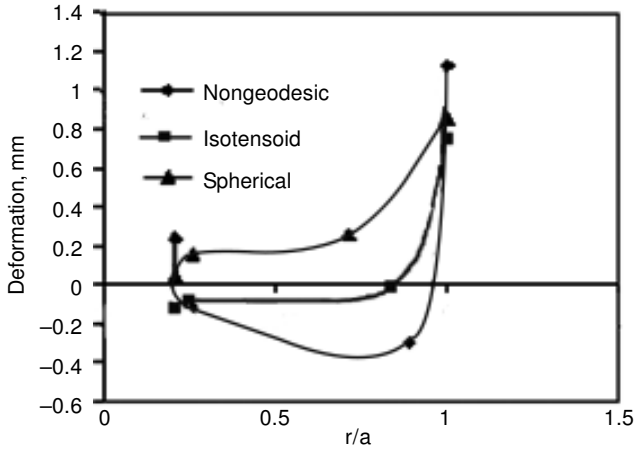

Figure 8 Radial deformations of end domes, mm

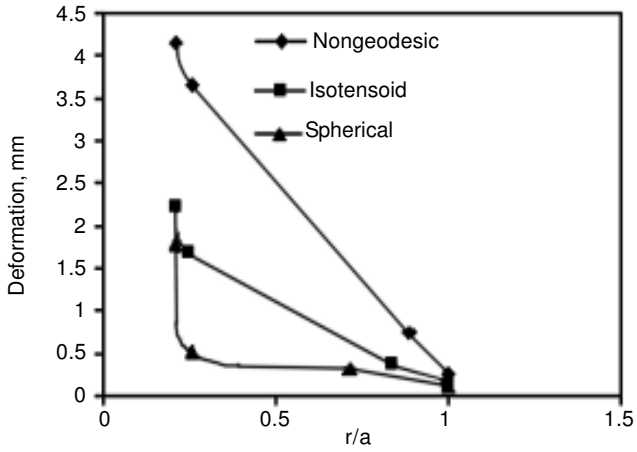

Figure 9 Axial deformations of end domes, mm

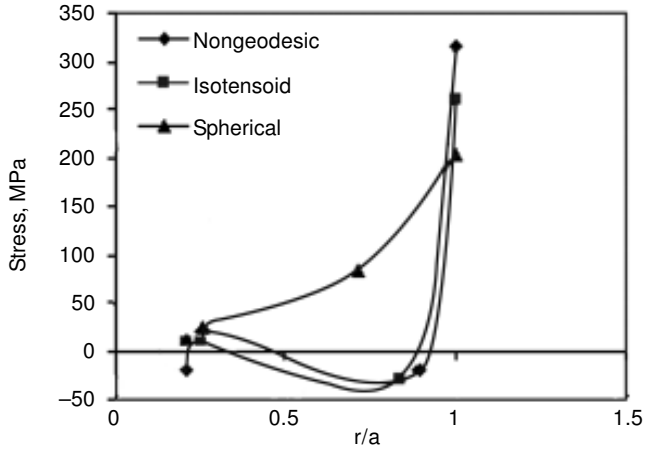

Figure 10 Axial stresses of end domes, MPa

down on the selection of correct end domes for the shell[14–15]. This study is obtained mainly to compare the structural behavior of the composite pressure vessel end domes. Shell 99, layered element is considered for the analysis of the structural behavior of the shell domes. The shell is subjected to uniform internal pressure of 7.5 MPa. The loading conditions are: $U_y = 0$ and $U_z = 0$ at the cylinder -end dome junction; whereas $U_x = 0$ and $U_z = 0$ at the pole opening.

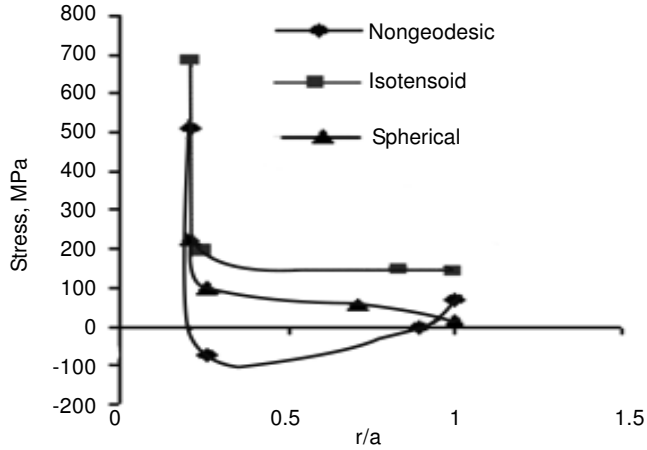

Figure 11 Stress along the fiber in the end domes, MPa

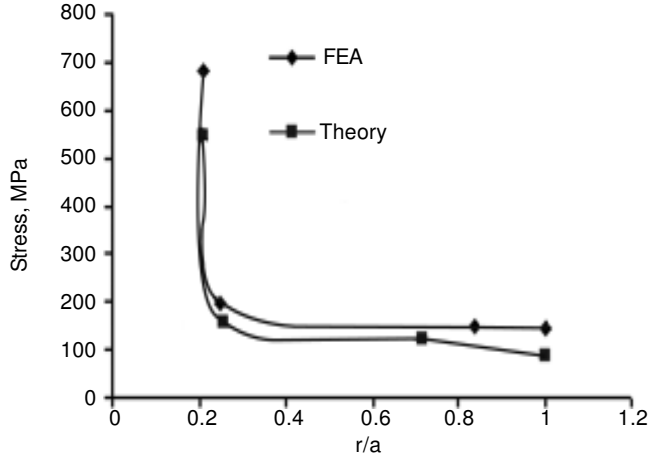

Figure 12 Stress along the fiber for an optimum end domes, MPa

Table 4 Resultant deformations and membrane stresses for end domes

End dome contours	Resultant deform-ation, mm	Max. axial stress, Mpa	Stress in the direction of the fiber, MPa
Hemispherical	1.873	214.02	255.023
Isotensoid	2.343	300.024	733.12
Non-geodesic	4.3	336.355	358.2

The angle of winding and the thickness through out the shell is considered to be varying[16–17]. Table 4 shows the list of the radial deformations and the various stresses in the dome contours. The angle of winding for the isotensoid and hemispherical end domes at the cylindrical -dome junction is calculated to be 12.14°, whereas for nongeodesic contour it is around 24.3°. The friction factor in case of non-geodesic (equation, 4) affects the angle of winding and thus the thickness of the shell. The maximum axial stress is noticed at the cylinder-end dome junction for all the three end domes. From the Table 1 to Table 3, it is clear that the thickness at the cylinder-end dome junction of non-geodesic dome is less compared to the other end domes leading maximum axial stresses for non-geodesic domes.

The radial deformations predicted by FEA shows that hemispherical end domes have less deformation compared to isotensoid and non-geodesic domes (Table 4). This can be due to their spherical shapes that remain fairly constant with pressurization. Non-geodesic end dome is subjected to higher deformation around 4.3 mm compared to isotensoid dome. It is mainly due to the non-linear behavior of the structure. The large deformation allows displacement adjustments as the shell are pressurized, which in turn, causes the shell to deflect more uniformly.

CONCLUSION

Iso-tensoid means having same tension along the length of the fibre direction. The FEA results indicate that the stress in the fibre direction for isotensoid is more uniform than other domes. Moreover the isotensoid end dome occupies less volume compared to other two end domes. In general if the pole opening size is increased; the thickness at the poles increases, which thereby leads to higher stress values at the poles. But this is not true with the isotensoid dome: for example-if the pole opening is increased from 125 mm to 335 mm, then the thickness of the hemi spherical shell increases by 25% and for that of isotensoid, more than 40% of thickness is reduced. The optimum dome takes different profiles for different pole openings, since the non-linear differential equation (3) possess the pole-opening radius as one of the parameters. It can be understood that isotensoid is an optimum end dome for developing composite pressure vessel.

REFERENCE

1. V A Bunakov and V D Protasov. 'Composite Pressure Vessels, Hand Book of Composites'. vol 2 Structure and Design, *Elsevier Science Publisher*, B V 1989.

2. R M Jones. 'Mechanics of Composite Materials'. *McGraw-Hill Co*.1975.

3. K Gramoll. 'Stress Analysis of Filament Wound Open-ended Composite Shells'. *34th Structural Dynamics and Materials Conference*, a Jolla CA; 1993.

4. J F Harvey. 'P E Theory and Design of Pressure Vessels'. *CBS Publishers and Distributors*.

5. S T Peters, W D Humphery and R F Foral. 'Filament Winding Composite Structure Fabrication, Second edition'. *SAMPE Publications*, 1999.

6. S S Kuo. 'Numerical Methods and Computers'. *Addison-Wesley Publishing Company*, 1966.

7. Cho-Chung Liang.Hung-Wen Chen, Chen-HuanWang. 'Optimum Design of Dome Contour for Filament-wound Composite Pressure Vessels based on ashape factor'. *Composite Structures*, vol 58, 2002.

8. G Lubin. 'Handbook of Composites'. *Van Nor strand Reinhold Co*., Inc; 1982; p 462.

9. Tae-Kyung Hwang, Chang-Sun Hong and Chun-Gon Kim. 'Size Effect on the Fibre Strength of Composite Pressure Vessels'. *Composite Structures,* vol 59, 2003, p 489.

10. Cheol-Ung Kim, I-Ho Kang, Chang-Sun Hong and Chun-Gon Kim. 'Optimal Design of Filament Wound Structures under Internal Pressure based on the Semi-geodesic Path Algorithm'. *Composite Structures*, vol 67, 2005, p 443.

11. R F Gibson. 'Principle of Composite Material Mechanics'. *Mc Graw Hill International Editions*,1994.

12. M Madhavi, Dr K V J Rao and Dr K N Rao. 'Material Characterization of Unidirectional High Strength Fibre Reinforced Composites using Filament Winding and Matched Die Mould Techniques'. *International Conference RAM 2008*, India, 2008.

13. D V Rosato and C S Grove. 'Filament Winding : Its Development, Manufacture, Applications and Design, In : Polymer Engineering and Technology'. *Interscience*, New York, 1964.

14. Carvalho, J D Lossie, D M Vandepitte and H Van Brussel'. 'Optimisation of Filament-wound Parts based on Non-geodesic Winding'. *Composites Manufacturing*, 1995.

15. Li, Xian-li and Lin,Dao-hai. 'Non-geodesic Winding Equation on a General Surface of Revolution'. *Proceedings of the 7th ICCM/ECCM Conference*, 1987.

16. A Gray. 'Modern Differential Geometry of Curves and Surfaces'. *CRC Press*, 1993.

17. G Mitchell. 'Non-geodesic Filament Winding Equation and Solution for Surfaces of Revolution, Intership report, Structures and Materials Laboratory'. *Faculty of Aerospace Engineering, Delft University of Technology*, Delft, July 2001.